



Published in final edited form as:

Cell Rep. 2022 July 12; 40(2): 111045. doi:10.1016/j.celrep.2022.111045.

Single-cell atlas of craniogenesis uncovers SOXC-dependent, highly proliferative, and myofibroblast-like osteodermal progenitors

Marco Angelozzi¹, Renata Pellegrino da Silva², Michael V. Gonzalez², Véronique Lefebvre^{1,3,*}

¹Division of Orthopaedics, Department of Surgery, Children's Hospital of Philadelphia, Philadelphia, PA, USA

²Center for Applied Genomics, Children's Hospital of Philadelphia, Philadelphia, PA, USA

³Lead contact

SUMMARY

The mammalian skull vault is essential to shape the head and protect the brain, but the cellular and molecular events underlying its development remain incompletely understood. Single-cell transcriptomic profiling from early to late mouse embryonic stages provides a detailed atlas of cranial lineages. It distinguishes various populations of progenitors and reveals a high expression of SOXC genes (encoding the SOX4, SOX11, and SOX12 transcription factors) early in development in actively proliferating and myofibroblast-like osteodermal progenitors. SOXC inactivation in these cells causes severe skull and skin underdevelopment due to the limited expansion of cell populations before and upon lineage commitment. SOXC genes enhance the expression of gene signatures conferring dynamic cellular and molecular properties, including actin cytoskeleton assembly, chromatin remodeling, and signaling pathway induction and responsiveness. These findings shed light onto craniogenic mechanisms and SOXC functions and suggest that similar mechanisms could decisively control many developmental, adult, pathological, and regenerative processes.

Graphical Abstract

This is an open access article under the CC BY-NC-ND license (<http://creativecommons.org/licenses/by-nc-nd/4.0/>).

*Correspondence: lefebvre1@chop.edu.

AUTHOR CONTRIBUTIONS

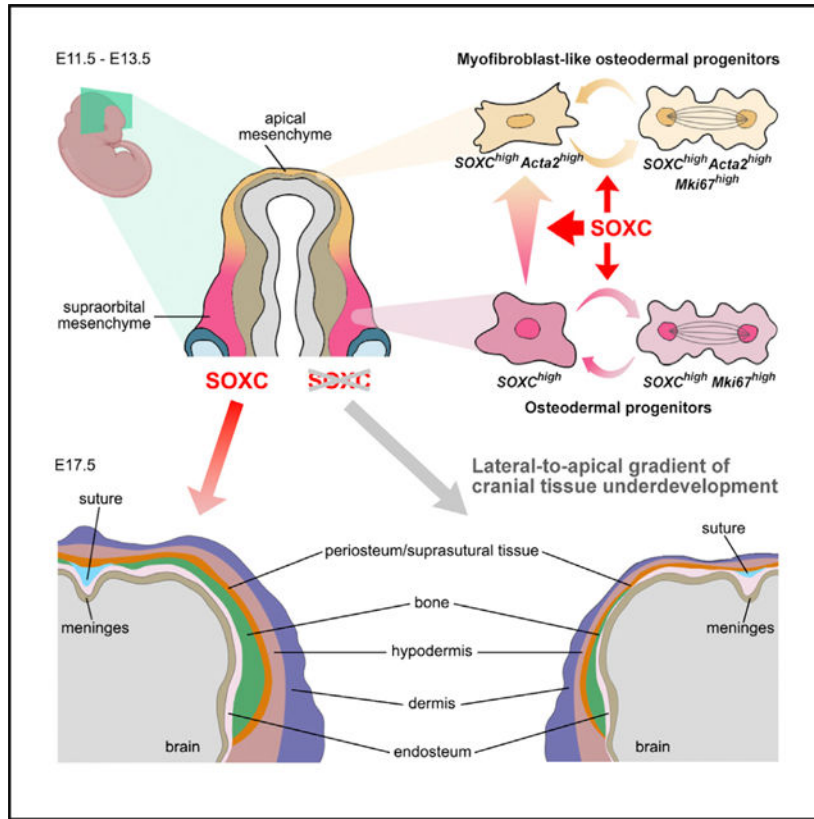
M.A. and V.L. conceived the research, designed the experiments, analyzed the data, and wrote the manuscript. M.V.G. and R.P.d.S. shared expertise in scRNA-seq assays and analyses. All of the authors approved the manuscript.

SUPPLEMENTAL INFORMATION

Supplemental information can be found online at <https://doi.org/10.1016/j.celrep.2022.111045>.

DECLARATION OF INTERESTS

The authors declare no competing interests.



In brief

Angelozzi and colleagues establish a detailed transcriptomic atlas of mouse embryonic craniogenesis and use mutant mice to show that SOXC (SOX4, SOX11, and SOX12 transcription factors) critically support osteogenesis and dermogenesis by promoting the expression of dynamic cellular and molecular properties of progenitor populations. SOXC could similarly affect many other processes.

INTRODUCTION

Craniogenesis is essential to vertebrates as it generates a skull vault and overlying skin to protect the brain and shape the head (Ishii et al., 2015). It is a paradigm developmental process whereby multiple progenitor and differentiated cell types coordinate spatiotemporal activities to generate functional tissues. Decades of research have uncovered key cellular and molecular mechanisms underlying craniogenesis, but more studies are needed to fully decipher these mechanisms and explain various forms of cranial dysplasias.

The skull vault comprises flat bones that intersect and expand in suture and fontanel joints (Morris-Kay and Wilkie, 2005). They form by intramembranous ossification—in other words, direct osteoblastogenesis of mesenchymal progenitors. Neural crest-derived cells form rostral cranial structures, including the frontal bone anterior part and the frontal and sagittal sutures, while paraxial mesoderm-derived cells generate caudal structures, including the frontal bone posterior part, parietal bones, and coronal suture (Jiang et al., 2002). At

mouse embryonic day 12.5 (E12.5), the two progenitor populations sit side by side in a supraorbital mesenchyme (SOM), while a thin mesenchyme already covers the entire brain. By E13.5, SOM cells greatly expand and migrate toward the lateral and apical head regions. Inner cells progressively commit to osteogenesis and outer cells to dermogenesis (Goodnough et al., 2016; Ting et al., 2009). By birth, all of the cranial tissues are specified, quickly expanding and maturing.

Defective craniogenesis causes various diseases (Richtsmeier and Flaherty, 2013; Tubbs et al., 2012). For instance, acalvaria (skull vault agenesis, with or without skin) likely results from osteodermal progenitor (ODP) anomalies, but its etiology remains unclear (Sharma et al., 2001). More commonly, craniosynostosis portrays premature suture and fontanel fusion, resulting in abnormal skull growth and shape. It generally occurs without other skeletal defects and is due to variants in genes that delay suture closure, including *FGFR1–3* (fibroblast growth factor receptors 1–3), *TWIST1*, and *MSX2* (basic-helix-loop-helix and homeobox transcription factors, respectively) (Lattanzi et al., 2017). In contrast, cleidocranial dysplasia (CCD) features delayed suture and fontanel closure, rudimentary clavicles, and short stature (Mundlos et al., 1997). It is due to heterozygous variants in *RUNX2* (RUNT-domain transcription factor-2, osteoblast determinant).

SOX4, SOX11, and SOX12 form the group C of SRY-box (SOX) transcription factors (Dy et al., 2008; Hoser et al., 2008; Kamachi and Kondoh, 2013). Most SOX proteins are master determinants of discrete cell types, such that the 20-member family specifies most cell lineages, and variants in SOX genes cause severe developmental diseases, called SOXopathies (Angelozzi and Lefebvre, 2019). For instance, heterozygous variants in *SOX2*, which specifies pluripotent and other stem cells, cause anophthalmia and microphthalmia. Heterozygous variants in *SOX9*, which specifies chondrocytes and Sertoli cells, cause campomelic dysplasia, a lethal skeletal malformation syndrome, and XY sex reversal. Whereas *SOX12* variants have not yet been linked to a disease, *SOX4* and *SOX11* heterozygous loss-of-function variants cause neurodevelopmental syndromes with various inconstant somatic defects, including craniosynostosis and mild craniofacial and digit dysmorphism (Angelozzi et al., 2022; Angelozzi and Lefebvre, 2019; Timberlake et al., 2019; Tsurusaki et al., 2014; Zawerton et al., 2019).

Studies in animal models have uncovered that SOXC are highly expressed in neuronal, mesenchymal, and other progenitor cells and control many developmental processes from early organogenesis onward (Bhattaram et al., 2010; Hoser et al., 2008; Schilham et al., 1996; Sock et al., 2004). Regarding skeletogenesis, *Sox11*^{-/-} mice are born with a cleft palate and underdeveloped skull and other bones (Sock et al., 2004). *Sox4*^{-/-} mice die *in utero* from heart malformation (Schilham et al., 1996), and *Sox4*^{+/-} mice look normal, but are osteopenic (Nissen-Meyer et al., 2007). Using conditional-null mice, we showed that SOXC have essential, largely redundant roles in limb buds to ensure skeletal progenitor survival and in fetal long bones to prevent perichondrium cells from undergoing chondrogenesis and to induce their secretion of signals required for cartilage growth and endochondral ossification (Bhattaram et al., 2014; Kato et al., 2015). *In vitro* studies have suggested that SOX4 and SOX11 may promote osteoblast progenitor proliferation and differentiation (Gadi et al., 2013; Nissen-Meyer et al., 2007). However, the osteogenic roles

of SOXC *in vivo* remain unknown. Regarding dermogenesis, *Sox4* and *Sox11* were found to be highly expressed in embryonic epidermal cells and re-expressed in postnatal skin wounds, where they re-activated an embryonic signature, including cytoskeleton genes driving cell motility (Miao et al., 2019). *Sox4* was also found to be expressed in hair follicle stem cells in adult mice and to help activate these cells during hair regeneration (Foronda et al., 2015). However, SOXC contribution to dermogenesis *in utero* remains unknown.

Here, we use single-cell transcriptome profiling assays (scRNA sequencing [scRNA-seq]) to better understand craniogenesis, and we combine these assays with analyses of SOXC mutant mice to study the SOXC contributions to this process. Our findings provide a detailed atlas of embryonic craniogenesis and uncover cell populations that rely on SOXC to deploy highly proliferative and myofibroblast-like properties and to overtly develop cranial tissues. We propose that SOXC may similarly empower other cell types in many processes.

RESULTS

SOXC are necessary for cranium overt development

To uncover how SOXC control craniogenesis, we generated mice harboring *Prx1Cre* (Logan et al., 2002) or *OsxCre* (Rodda and McMahon, 2006) and SOXC conditional-null alleles (Bhattaram et al., 2010; Dy et al., 2008). We first verified the Cre transgene spatiotemporal activities using *R26^{tdT}*, an allele constitutively expressing tandem-dimer Tomato (tdT) upon Cre recombination (Madisen et al., 2010). As reported (Dasgupta et al., 2019; Rodda and McMahon, 2006; Seo and Serra, 2009; Takarada et al., 2016), *Prx1Cre* targeted mesoderm-derived cells and some neural crest-derived cells in frontal bone, parietal bone, suture, dermal, and meningeal primordia by as early as E11.5, and *OsxCre* targeted osteoblastic cells, starting at approximately E13.5 (Figures S1A–S1C).

Skeletal staining at E18.5 (1 day before birth) showed, as reported (Bhattaram et al., 2014), that *Sox4^{fl/fl}Sox11^{fl/fl}Sox12^{fl/fl}Prx1Cre* (*SOXC^{Prx1Cre}*) fetuses had severely malformed limbs and no sternum (Figure S2A). Moreover, parietal bones and frontal bone caudal parts were mineralized laterally but not apically, and interparietal and supraoccipital bones seemed largely missing (Figure 1A). Single SOXC mutants looked normal (Figure S2B), except that *Sox4^{Prx1Cre}* and *Sox11^{Prx1Cre}* parietal and frontal bone apices were partially undermineralized (Figure 1B). Inactivation of all but one SOXC allele caused milder defects when the intact allele was from *Sox11* or *Sox4* rather than *Sox12* (Figures S2C and S2D). *OsxCre* newborn mice had fenestrated skull bones, as described (Huang and Olsen, 2015; Wang et al., 2015) (Figure 1C). In addition, *SOXC^{OsxCre}* mice had slightly undermineralized frontal and parietal bone apices (Figure 1D). Histological analysis revealed that E18.5 *SOXC^{Prx1Cre}* fetuses had underdeveloped parietal bone apices, as expected, and also had lateral thinning of these bones, an underdeveloped sagittal suture, and apical hypoplasia of hypodermis and dermis (Figure 1E). Cranial tissues appeared normal in *OsxCre* mice and slightly underdeveloped in *SOXC^{OsxCre}* mice (Figures 1F and 1G). Altogether, these data indicated that SOXC, in particular *Sox4* and *Sox11*, are necessary for proper craniogenesis and likely have additive and redundant functions in ODPs.

Generation of a transcriptomic atlas of embryonic craniogenesis

We characterized cranial cell populations in *SOXC^{Prrx1Cre}* and control littermates by scRNA-seq at five developmental stages (Figure S3A): E11.5, E12.5, and E13.5, when progenitor cells cover the head, develop within and migrate out of the SOM, and commit to specific lineages; and E15.5 and E17.5, when cranial cells span a spectrum of progenitor to differentiated states (Ishii et al., 2015). We included all cranial tissues (but rostral parts) because of tight associations between skeletal, dermal, and meningeal cells, but excluded the abundant dermis at E17.5. We profiled $13,249 \pm 2,120$ cells per stage and genotype, and detected $1,641 \pm 931$ expressed genes per cell. Uniform manifold approximation and projection (UMAP) dimensional reduction of all samples combined identified 22 cell clusters (Figure S3B; Table S1). Twelve clusters were negative or weak for *Prrx1* (paired-related homeobox transcription factor-1; promoter used to generate *Prrx1Cre*) expression and comprised non-craniogenic cells (Figures S3C–S3E). The other 10 clusters expressed *Prrx1* moderately to highly. Upon re-clustering them, regressing out cell-cycle genes, we obtained 17 populations (Figure S3F). C1–C3 likely comprised ODPs, as they highly expressed mesenchymal markers (e.g., *Prrx1*, *Twist1*, *Fnl1* [fibronectin]) and weakly expressed the dermal determinant *Twist2* and osteogenic determinants *Runx2* and *Dlx5* (distal-less homeobox transcription factor-5) (Figure S3G; Table S2). C4 and C5 comprised pre-osteoblasts and osteoblasts, respectively. Both strongly expressed *Runx2*. C4 more strongly expressed *Dlx5*, and C5 more strongly expressed *Sp7* (osteoblast determinant). C6 and C7 likely contained dermal and hypodermal cells, more highly expressing *Twist2* and *Dlk1* (Delta-like notch ligand-1), respectively. C8 likely comprised osteomeningeal cells, expressing mesenchymal markers along with *Foxd1* (Fork-head-box transcription factor-D1; meningeal determinant), *Runx2*, and *Sox9* (SRY-box transcription factor-9, chondrogenic determinant). C9–C12 contained meningeal cells, highly expressing *Foxd1* and primary meninx, pial, dural, and arachnoid markers (Dasgupta and Jeong, 2019; DeSisto et al., 2020). C13 and C14 comprised chondroblasts and chondrocytes, respectively. Both expressed *Sox9*, *Col2a1* (collagen-2), and *Acan* (aggrecan), but C14 more strongly expressed them. C15 contained pericytes, highly expressing *Rgs5* (regulator of G protein signaling 5) and *Kcnj8* (inwardly rectifying K⁺ channel-8), and C16 and C17 likely comprised cell doublets.

Since *SOXC^{Prrx1Cre}* embryos had skull and dermis defects, we focused our study on C1–C8. Refined clustering (regressing out cell-cycle effects) generated 17 populations, each original cluster being split into one to three new ones (Figure 2A). For instance, C1 split into C1.1, C1.2, and C1.3; C2 remained intact; and C3 split into C3.1 and C3.2. C1.1 and C1.2 contained ODPs originating at >40% from E11.5, ~40% from E12.5, <10% from E13.5, and <10% from E15.5 and E17.5 (Figures 2B and 2C). They had similar gene signatures, but C1.1 was discreetly proliferative and C1.2 was highly proliferative, as inferred by expression levels of genes such as *Mki67* (Ki67) and *Top2a* (DNA topoisomerase-2 α) (Figure 2D; Table S3). They thus likely contained early ODPs differing by cell-cycle status.

C1.3 and C2 contained 20%–30% cells from each of the E11.5–E13.5 stages and 10%–20% cells from the E15.5 and E17.5 stages combined. They thus persisted longer than C1.1/C1.2. In addition to expressing ODP markers, they displayed a hitherto unknown

myofibroblast-like signature (Pakshir et al., 2020), branded by high expression of *Acta2* (smooth muscle actin- α 2) and *Tagln* (transgelin), as well as *Msx2* (MSH-homeobox transcription factor, osteoprogenitor regulator). While C1.3 cells were very proliferative, C2 cells were not, and their myofibroblast-like signature was supported by the upregulation of sterol biosynthesis genes such as *Hmgcs1* (hydroxymethylglutaryl-coenzyme A [HMG-CoA]-synthase-1) and *Msmo1* (methylsterol monooxygenase-1). We deduced that C1.3 and C2 contained intermediate ODPs, endowed with myofibroblastic features, but differing in cycling status.

C3.1 and C3.2 contained ODPs that overtly developed after E12.5 and E13.5, respectively, and thrived by E17.5. They highly expressed *Sfrp2* (secreted frizzled-related protein-2) and *Meox2* (mesenchyme homeobox-2). *Sfrp2* promotes fibroblast activity and marks sutures and periosteum (Holmes et al., 2020). *Meox2* arrests cell growth and changes myofibroblasts to fibroblasts (Cunnington et al., 2014). Accordingly, C3.1 and C3.2 weakly expressed proliferation and myofibroblast markers, and highly expressed osteogenic and hypodermal markers such as *Aspn* (asporin) and *Thbs2* (thrombospondin-2). C3.1 was positive for *Tac1* (tachykinin-1) expression, marking cells between periosteum and dura (Kosaras et al., 2009; Wang et al., 2021). C3.2 surpassed C3.1 in expressing *Col8a1*, *Fbln2* (fibulin-2), *Igfbp3* (insulin-like growth factor-binding protein-3), and other periosteal and neonatal suture markers (Holmes et al., 2020). C3.1 and C3.2 thus likely contained late ODPs in periosteum and sutures.

As expected, C4 preosteoblasts highly expressed early osteoblast markers such as *Postn* (periostin), while C5 cells more highly expressed mature markers such as *Bglap* (osteocalcin) and *Dmp1* (dentin matrix acidic phosphoprotein-1). C4 arose by E12.5 and C5 by E15.5, and both enlarged through E17.5.

C6 and C7 divided into C6.1–C6.3, C6/7, C7.1, and C7.2. All of them appeared by E12.5 and greatly enlarged by E15.5, except C7.2, which arose by E15.5 (most C6 and some C7 cells were omitted in E17.5 scRNA-seq). All 6 clusters distinguishingly expressed dermal/hypodermal markers, such as *Osr2* (odd-skipped-related transcription factor-2) and *Egfl6* (epidermal growth factor-like-6). C6.1–C6.3 contained dermal cells, being still positive for *Twist1* and strongly expressing *Twist2* and *Tcf4* (transcription factor-4). C6.1 and C6.2 similarly expressed fibroblast markers such as *Fnl1*, *Irx1* (Iroquois homeobox protein-1), and *Vcan* (versican), and likely corresponded to dermal cells at non-proliferative and highly proliferative stages, respectively. C6.3 corresponded to dermal papilla cells, marked by the expression of *Trps1* (transcriptional repressor GATA-binding-1) and *Cpne5* (copine-5). C7.1 and C7.2 expressed markers described for hypodermis, periosteum, and sutures such as *Dlk1*, *Meox2*, *Sfrp2*, and *Clec3b* (tetranectin) (Driskell et al., 2013; Holmes et al., 2020). C7.1 also expressed progenitor markers such as *Twist1*, *Twist2*, and *Ly6a* (stem cell antigen-6), and uniquely expressed *Ccn3* (cellular communication network factor-3), whose expression pattern in craniogenesis is unknown. C7.2 highly expressed tenocyte markers, such as *Eln* (elastin), *Scx* (scleraxis), and *Tnmd* (tenomodulin). C7.1 and C7.2 could thus contain periosteal/perisutural hypodermal-like cells with progenitor and tenocytic features, respectively. With a phenotype overlapping that of C6 and C7, C6/7 likely contained hypodermal cells.

C8 split into three clusters. C8.1 and C8.2 were present at all of the stages and were weakly proliferative. C8.1 was more positive for *Runx2* and *Postn* than C8.2 and less positive for *Foxd1*, suggesting that these clusters represented osteomeningeal layers located closer to the bone and meninges, respectively. C8.3 arose at approximately E13.5 and was largest at E17.5 and growth arrested. It could thus contain more mature cells than C8.1 and C8.2. The three clusters shared with C7.2 a high expression of *Coll4a1* and *Ecrq4* (augurin precursor, proliferation inhibitor).

Sox4 and *Sox11* were most highly expressed at E11.5 and E12.5 (Figure 2E). *Sox4* expression was fairly even among progenitor and differentiated clusters, while *Sox11* was most strongly expressed in C1.1/C1.2 and C6.1/C6.3 and was a top 20 marker of C1.1 early ODPs and C6.3 dermal condensates. Both genes were downregulated gradually over time, even in cell clusters arising after E12.5, such that few cells still expressed them at E17.5. *Sox12* expression followed a similar pattern, but was always weak.

In line with these data, RNA velocity and pseudotime analyses suggested that some C1.1/C1.2 early ODPs gave rise to C1.3/C2 intermediate ODPs, themselves generating in cascade C3.1 late and C3.2 very late ODPs (Figures 2F and 2G). They also suggested that C1/C2 ODPs, and possibly some C3.1 late ODPs and C8.3 osteomeningeal cells, gave rise to C4 preosteoblasts, which then turned into C5 osteoblasts. C7.1 and C7.2 periosteum/suture-associated hypodermal cells appeared to arise from C1, C2, and C3 ODPs. C6.1/C6.2 dermal and C6/7 hypodermal cells likely derived from C1/C2 ODPs, and C6.1/C6.2 cells likely generated C6.3 cells. C8 cells appeared to arise independently of the osteo/dermal cells.

In summary, our atlas of embryonic cranial cells identified a large spectrum of progenitor and differentiated cell types belonging to osteogenic, dermal, meningeal, and other lineages, and revealed that SOXC are expressed in all cells, but most prominently in early progenitors.

Spatial mapping and refined identification of embryonic cranial populations

We conducted RNA *in situ* hybridization assays (RISH) for cluster-enriched markers to spatially map and more definitively identify atlas populations. At E11.5, C1.1/C1.2 early ODPs (*Sox4^{high}Sox11^{high}Mki67^{low/high}Tagln^{low}Runx2^{low}Twist2^{low}Foxd1^{low}*) were populating the SOM region, and thin layers of apparently mixed C1.3/C2 intermediate ODPs and C8.1/8.2 osteomeningeal cells (*Sox4^{high}Sox11^{med}Mki67^{high/med}Tagln^{high/med}Runx2^{low}Twist2^{med}Foxd1^{med/high}*) formed the lateral (LM) and apical (AM) mesenchyme (Figures 3A and S4A). In the SOM and LM, some C1/C2 cells were starting to form *Twist2^{high}* outer and *Runx2^{high}* inner populations, presaging dermal and osteoblastic commitment, respectively. Similar patterns were seen at E12.5 (Figures 3B and S4B), except that the *Runx2^{high}* and *Twist2^{high}* populations were largely distinct in the SOM/LM region, reflecting transition into C4 preosteoblasts and C6.1/C6.2 dermal cells, respectively. The AM had an outer C1.3/C2 layer and an inner meningeal/C8 osteomeningeal layer.

By E13.5, C4/C5 cells (*Runx2^{high}*) and C6.1–C6/7 cells (*Twist2^{high}*) were developing parietal bone and skin primordia in the SOM/LM region (Figures 3C and S4C). They were parted by a streak of C1.3/C2 cells. C7.1 hypodermal-like periosteal/perisutural

progenitors (*Sox4^{high} Tagln^{med} Egfl6^{high} Ccn3^{high} Sfrp2^{high} Col8a1^{high} Msx2^{low} Tac1^{low}*) were starting to line bone tissue. The cells located at the interface of the bone and brain tissues were similar, but *Foxd1^{high} Col14a1^{high} Col8a1^{neg}*. They thus identified as meningeal and C8 osteomeningeal cells. The AM further split into an outer layer of C6.1/C6.2/C6.7 hypo/dermal cells (*Twist2^{high} Egfl6^{high}*), a middle layer of C1.3/C2 cells becoming C3.1 late ODPs in nascent suture and bone (*Runx2^{med} Msx2^{high} Sfrp2^{high} Tac1^{high} Col8a1^{high}*), and inner layers of osteomeningeal (*Foxd1^{high} Msx2^{high} Col14a1^{high} Col8a1^{high} Tagln^{med} Sfrp2^{med}*) and meningeal cells.

Cranial tissues greatly expanded and matured by E15.5 and E17.5 (Figures 3D, S4D, and S5). *Sox4* and *Sox11* were expressed weakly in most cranial cells, but strongly in nascent C6.3 dermal papillae. C6.1/C6.2 cells (*Twist2^{high} Egfl6^{high} Dlk1^{low} Col14a1^{low}*) and C6.7 cells (*Twist2^{med} Egfl6^{high} Dlk1^{high} Col14a1^{med}*) formed several dermal and hypodermal layers, respectively. Thin but dense periosteal and perisutural tissues contained C7.1 cells (*Ccn3^{high}*), C3.2 very late ODPs, and C7.2 tenocytic cells (*Dlk1^{high} Col14a1^{high} Col8a1^{high} Tnmd^{high}*). The parietal bone was rich in C5 osteoblasts (*Runx2^{high} Sp7^{high} Msx2^{neg}*) in its lateral base, but its apical side and the suture core remained immature, apparently containing C4 preosteoblasts, C3.1 late ODPs (*Runx2^{high} Sp7^{low} Foxd1^{med} Tagln^{low} Msx2^{high}*), and C1.3/C2 cells (*Tagln^{high}*).

SOXC promote the generation of highly proliferating and myofibroblast-like ODPs, as well as downstream cell types

SOXC^{Prx1Cre} cranial cells formed the same clusters as control cells (Figure 4A) and RNA velocity and cell trajectory patterns suggested that their lineage decisions were not drastically altered (Figures 4B and S5A). Differences were nonetheless detected in the relative sizes of clusters. In particular, the C1 and C2 ODP clusters were smaller in mutants than controls at E11.5 and E12.5 (Figure 4C), due to reduced proportions of C1.2 highly proliferating and C1.3/C2 myofibroblast-like cells. At E13.5, the C1.3/C2:C1.1/C1.2 ratio was reduced by half in mutants versus controls, hinting that SOXC promoted the acquisition of the myofibroblast-like signature. Even so, mutant ODPs seemed to convert as fast as controls into C6.1–C6.7 dermal and hypodermal cells and slightly faster into C4/C5 osteoblastic cells and C7.1 periosteal/perisutural cells. At E15.5, C6.1–C6.7 cells accounted for every other control cranial cell, but for 5-fold fewer mutant cells, suggesting a major expansion defect of mutant cells. Exclusion of these cells from analyses at E15.5 and E17.5 helped reveal that C3 late ODPs were overrepresented in mutants, possibly because by then C4/C5 and C7 cells were not developing as fast as in controls (Figure 4D). SOXC may thus promote expression of the ODP myofibroblast-like signature and amplification of progenitor and downstream cell types.

SOXC upregulate genes conferring ODPs with dynamic properties

Since ODPs were *SOXC^{high}* in E11.5–E13.5 controls and were impaired in mutants, we analyzed the SOXC dependency of their transcriptomes. SOXC loss resulted in a significant downregulation of 471 genes, most at E13.5 (373, 79%) (Figure 5A; Table S4A). These genes fell into five groups based on temporal expression (Figure 5B). Group 1 contained *Sox4*, *Sox12*, and 113 other genes most highly expressed at E11.5–E13.5,

and group 2 contained *Sox11* and 56 other genes most highly expressed at E11.5 and E12.5. Many of these genes depended on SOXC for early-stage upregulation. Groups 3 and 5 comprised 74 and 47 genes, respectively, whose expression increased over time and was most dependent on SOXC at E13.5. Group 4 contained 178 genes that relied on SOXC for striking upregulation at E13.5. The genes downregulated in E11.5 and E12.5 SOXC mutants belonged mostly to groups 1 and 2, whereas those downregulated at E13.5 belonged to all groups (Figure 5C). Gene Ontology (GO) analysis for all and individual groups suggested that SOXC primarily upregulated genes involved in actin filament organization (e.g., *Acta2*, *Tagln*) and associated processes such as cell adhesion and migration (Figures 5D and S6B; Table S4B). SOXC also appeared to upregulate genes involved in chromatin remodeling and transcription (e.g., *Smarca1*, SWI/SNF-related, actin-dependent chromatin regulator; *Hmgb3*, HMG-box protein-3; *Tead2*, TEA-domain transcription factor-2; *Ezh2*, polycomb repressive complex-2 component), sterol biosynthesis (e.g., *Hmgcs1*), and signaling pathways regulating craniogenesis (e.g., *Mdk*, Midkine; *Wls*, WNT-ligand secretion mediator; *Epha7*, ephrin receptor-7; *Cxcl14*, CXC-motif cytokine-14). Cell proliferation was a mildly significant category, and its downregulated genes encoded signaling and extracellular matrix components (e.g., *Mdk*, *Dlk1*, *Tnmd*, *Thbs1*), and only a few cell-cycle regulators (e.g., *Cdc42*), suggesting that SOXC may control cell proliferation indirectly more than directly.

C1/C2 mutants upregulated 282 genes, most at E13.5 (193, 68%) (Figure 5E; Table S4A). These genes fell into three groups (Figure 5F). Group 1 contained 139 genes most highly expressed at E11.5 and E12.5 in controls, and still highly expressed in mutants at E13.5 (Figures 5F and 5G). Group 2 contained 102 genes most strongly expressed in controls at E15.5 and E17.5 and already upregulated in mutants at E13.5. Group 3 contained 38 genes transiently upregulated at one or another time point in controls, and differentially upregulated in mutants. GO analysis for all and individual groups identified gene categories related to ribosome formation and protein translation (e.g., *Rpl28*, ribosomal protein-L28), mesenchyme development, ossification, and cell proliferation (e.g., *Alx1*, aristaless-like homeobox-1; *Coll1a1*; *Postn*; *Ccnd1*, cyclin-D1), suggesting that SOXC may limit translation and other activities typical of differentiated cells (Figures 5H and S6C; Table S4C).

We used RISH to validate the downregulation of key genes. As expected, *Sox4* and *Sox11* were already drastically downregulated in the SOM, LM, and AM of E11.5 *SOXC^{Ptx1Cre}* embryos (Figures 6A, 6B, and S7A). In groups 1 and 2, *Mdk*, *Hmgb3*, *Tead2*, *Ezh2*, and *Hmgcs1* were highly expressed in the SOM, LM, and AM of control embryos, and all of them were strongly downregulated in mutants by E11.5, except *Hmgcs1*, which appeared downregulated only by E13.5, as in scRNA-seq. In group 4, the myofibroblastic cytoskeleton genes *Acta2*, *Tagln*, and *My19* showed reductions in both expressing cell numbers and expression level per cell from E11.5 to E15.5 (Figures 6C and S7B). Similar findings were made for regulatory genes such as *Twist1*, *Msx2*, and *Cxcl14*.

Altogether, these data suggested that SOXC help progenitor cells execute dynamic cellular and molecular activities, including actin cytoskeleton formation and cell proliferation, adhesion, and motility, and retard the upregulation of genes involved in overt tissue morphogenesis.

SOXC promote cranial tissue morphogenesis by stimulating cell proliferation

We asked whether the underdevelopment of cranial structures in *SOXC*^{Prx1Cre} embryos involved inapt cell differentiation, survival, or proliferation. scRNA-seq assays showed that cell specification and differentiation markers were expressed at normal or partially reduced levels in mutant clusters (Figure 7A). RISH at E13.5–E17.5 confirmed these data and showed that each cell type developed in mutants where expected, but was represented by fewer cells, especially in the head apex (Figures 7B and S8). For instance, mutants had fewer *Twist2*⁺*Egfl6*⁺ dermal cells and fewer *Egfl6*⁺ cells surrounding dermal papillae. Mutant *Ccn3*⁺ and *Tnmd*⁺ cells were sparse rather than packed in periosteal and sutural structures. Similarly, *Runx2*⁺*Sfrp2*⁺ osteogenic cells were present in limited numbers in mutant sutures and *Runx2*⁺*Dmp1*⁺ osteoblasts in parietal bones. Thus, SOXC promote the amplification of cell populations before or during differentiation, but they may not control lineage specification and tissue patterning.

TUNEL assays detected equally low numbers of apoptotic cells in E11.5–E15.5 control and mutant crania (Figure S9A). In contrast, 5-ethynyl-2'-deoxyuridine (EdU) incorporation assays and phospho-histone-3 immunostaining assays showed lower percentages of proliferating cells in the SOM/LM but not in the AM at E13.5, and in all cranial tissues at E14.5 and E15.5 (Figures 7C and S9B–S9D). SOXC thus stimulate the proliferation of progenitor and differentiating cranial cells.

DISCUSSION

This study expands the current knowledge of cellular and molecular mechanisms driving craniogenesis. It provides a detailed atlas of the cell types participating in this process during mouse gestation and reveals key roles for SOXC genes. In particular, it identifies a myofibroblast-like signature in intermediate ODPs that likely confers important cell properties. SOXC ensure the overt development of skull bones, sutures, and cranial dermis, especially in the head apex. They promote the expression of the myofibroblast-like signature, cell proliferation, and other dynamic activities, but neither lineage specification nor differentiation. These mechanisms may apply to many processes involving myofibroblastic and highly proliferative cells.

Our transcriptomic atlas encompasses all cranial cells at five milestone embryonic stages. It reveals a large spectrum of interconnected progenitor populations committing progressively to the skeletal, dermal, and meningeal lineages. It thus significantly complements datasets published for discrete populations at one or two time points, such as E15.5–E18.5 suture cells (Farmer et al., 2021; Holmes et al., 2020), E14 meningeal fibroblasts (DeSisto et al., 2020), and E14.5 back skin progenitors (Sennett et al., 2015). The major findings of our atlas analysis include the following.

Early and intermediate ODPs clustered in four populations differing primarily in cell proliferation and actin cytoskeleton gene expression. These populations thus likely represented progenitors at different activity levels rather than progenitors with different origins or fates. Spatial mapping showed highly proliferating ODPs in the SOM, LM, and AM, indicating that the cells continue to replicate in all locations as the head rapidly grows

and as they prepare to commit to specific lineages. Unlike progenitors in the SOM, those located in the LM and AM highly expressed myofibroblast-specific cytoskeleton genes (e.g., *Acta2*, *Tagln*, *Myl9*). To our knowledge, this gene signature has not been described previously in craniogenesis. However, it was shown to be critical for cell proliferation, adhesion to tissue matrix, contractility, and migration in various biological events, including midface development and ventral midline closure (Aldeiri et al., 2017; Svitkina, 2018; Vasudevan and Soriano, 2014). By analogy, we speculate that myofibroblastic properties help ODPs achieve their well-documented migration from the SOM to other head regions (Ishii et al., 2015), proliferate, and maintain the integrity of their tissue coverage around the fast-enlarging head.

We confirmed that meningeal cells derive, like dermal and osteogenic cells, from *Prrx1^{high}* mesenchymal progenitors (Jiang et al., 2002), and we revealed a population of hypodermal-like periosteal/perisutural cells that uniquely expresses *Ccn3*. *Ccn3*-null mice have no major skeletal defects (Canalis et al., 2010), but readily regenerate bone, likely because the matricellular protein CCN3 inhibits bone morphogenetic protein (BMP)-driven osteogenesis (Matsushita et al., 2013). CCN3 may thus help repress osteogenesis in bone-flanking cells. Tenocyte-like cells, namely expressing *Tnmd*, were recently shown to cover the fetal coronal suture (Farmer et al., 2021). We confirmed the existence of this *Tnmd^{high}* population and found that it was both suprasutural and periosteal. It may thus provide mechanical resistance and sensation to sutures (Farmer et al., 2021) and to nascent skull bones.

Other than delivering a detailed atlas, our study identified important SOXC contributions to craniogenesis. We found *Sox4* and *Sox11* expression to be widespread and strong at E11.5, but to fade over time, such that few cells were still positive at E17.5. *Sox12* expression was low at all stages. These data align with those of many studies that showed key, redundant roles for *Sox4* and *Sox11* in various progenitor cell types in embryos and little to no *Sox12* contribution. Our data also validated *in vitro* findings that *Sox4* and *Sox11* sustain osteogenic cell proliferation, but did not validate that SOXC promote *Runx2* and *Sp7* activation and thereby osteoblastogenesis (Gadi et al., 2013; Nissen-Meyer et al., 2007; Yu et al., 2020). SOXC-deficient cranial progenitors indeed timely started to express both genes and to form bone in the lateral sides of the skull. Skeletal staining showed that apical bone formation was impaired in SOXC mutants, but histology and *in situ* analyses showed that this defect was due to cell paucity rather than to lineage specification and differentiation issues. SOXC may thus promote osteoblastogenesis *in vitro* as a result of activities in progenitors rather than in differentiating cells. The fact that *SOXC^{OsxCre}* skulls were less affected than *SOXC^{Prx1Cre}* skulls supports this proposition. An alternative or complementary explanation could be that dermal and osteogenic cells, both of which were affected in *SOXC^{Prx1Cre}* mutants, reciprocally control their differentiation, as previously proposed (Tran et al., 2010), and that their crosstalk is SOXC dependent, as proposed for perichondrium cells and chondrocytes (Kato et al., 2015) and as supported by our finding that SOXC are necessary to upregulate many signaling pathway genes.

Many studies found SOXC necessary for progenitor cell survival in early development, such that cell death prevented the assessment of other SOXC functions. We showed this, for instance, in branchial arch and limb bud mesenchyme in E11.5 SOXC-deficient embryos

(Bhattaram et al., 2010). In the present study, however, we did not detect an increase in cell death in *SOXC^{Prx1Cre}* crania at E11.5 or E12.5. We do not know whether this difference relates to differential spatial, temporal, or other conditions. Instead, we found *SOXC^{Prx1Cre}* cranial cells to be less proliferative at and after E13.5. This defect likely explains the reduced number of cell layers making up these crania. However, since this defect did not become significant until SOXC expression started to decline, and since few genes directly regulating cell-cycle progression were differentially expressed in *SOXC^{Prx1Cre}* cells, we gather that SOXC promote cell proliferation mainly indirectly.

Actin cytoskeleton assembly and related cellular activities were pathway categories most represented by the genes downregulated in *SOXC^{Prx1Cre}* ODPs, and key cytoskeleton component and regulatory genes were among the most affected genes. A weakened cytoskeleton thus likely contributed to the cranial defects of *SOXC^{Prx1Cre}* embryos. It may likewise explain defects occurring in other processes upon SOXC loss, but still unsolved molecularly. Developmental processes may include midface development and ventral midline closure, which are SOXC dependent (Bhattaram et al., 2010; Sock et al., 2004) and involve a myofibroblastic signature. They may also include heart malformations resulting from impaired neural crest cell proliferation and migration upon SOXC loss (Huang et al., 2016; Paul et al., 2014). Beyond development, processes may include synovial hyperplasia, shown to be SOXC dependent in a mouse model of rheumatoid arthritis (Bhattaram et al., 2018), and aggressiveness and metastatic behavior of various cancers linked to SOXC overexpression (Moreno, 2020; Tsang et al., 2020; Yoshida, 2020). Cytoskeleton-related genes are certainly not the only genes controlled by SOXC. Our data identified genes involved in epigenetic and transcriptional regulation (e.g., *Ezh2*, *Hmgb3*, *Msx2*) and in growth factor and signaling pathways (e.g., *Mdk*, *Cxcl14*), suggesting roles for SOXC in various progenitor activities, including chromatin remodeling and production of and responses to regulatory signals.

In conclusion, our transcriptomic atlas and finding that SOXC significantly contribute to craniogenesis, likely by controlling the actin cytoskeleton and related activities such as cell proliferation and migration, greatly increase our current cellular and molecular understanding of craniogenesis. They will likely motivate and illuminate new investigations to further elucidate developmental, adult, pathological, and regenerative events in many processes.

Limitations of the study

A limitation of our study is its use of *Prx1Cre* to inactivate SOXC in mice. The transgene effectively targets mesoderm-derived cranial progenitors, but only target a subset of neural crest-derived cranial progenitors. Thus, although we omitted cranial regions derived from the neural crest, we may have underestimated the impact of SOXC on craniogenesis. Furthermore, since *Prx1Cre* and the SOXC genes are active in multipotent progenitors, our strategy did not differentiate the cell-autonomous from the non-cell-autonomous roles of SOXC. Another limitation is that we did not identify the direct SOXC targets. Previous studies provided strong evidence that *Tead2* and *Ezh2* are direct SOXC targets (Bhattaram

et al., 2010; Tiwari et al., 2013). We predict that other genes, also downregulated in *SOXC^{Prx1Cre}* ODPs, are direct SOXC targets.

STAR★METHODS

RESOURCE AVAILABILITY

Lead contact—Further information and requests for resources and reagents should be directed to Véronique Lefebvre (lefebvre1@chop.edu).

Materials availability—This study did not generate unique reagents.

Data and code availability—The scRNA-seq data have been deposited at NCBI Gene Expression Omnibus and are publicly available as of the date of publication (GSE174716).

This paper does not report original code. Additional information required to reanalyze data reported in this paper is available from the lead contact upon request.

EXPERIMENTAL MODEL

Mice—Mice were used as approved by the Children’s Hospital of Philadelphia Institutional Animal Care and Use Committee. Mice carrying *Sox4*, *Sox11* and *Sox12* conditional null alleles (*Sox4^{fl/fl}*, *Sox11^{fl/fl}* and *Sox12^{fl/fl}*, respectively) were previously generated by flanking the entire coding sequences of the SOXC genes with loxP sites (Bhattaram et al., 2010; Penzo-Mendez et al., 2007). Single, compound and triple SOXC mutant mice were generated using previously described *Prx1Cre* (Logan et al., 2002) or *OsxCre* (Rodda and McMahon, 2006) transgenes. For embryo generation, dams were checked for the presence of vaginal plugs the morning after mating. Noon on the day of plug visualization was considered as embryonic day 0.5 (E0.5).

METHOD DETAILS

Whole-mount skeletal staining—Whole-mount skeletal staining was performed as previously described (Rigueur and Lyons, 2014). Briefly, E18.5 fetuses were euthanized by hypothermia in ice-cold PBS, and newborn pups (at postnatal day 0, P0) were euthanized by hypothermia in a plastic bag placed in wet ice. Specimens were then scalded in hot tap water. After removal of the eyes, skin and internal organs, carcasses were fixed in 95% ethanol overnight, followed by acetone overnight. They were then incubated in a 0.03% Alcian Blue solution in 80% ethanol and 20% glacial acetic acid overnight to stain cartilage, and washed with ethanol and 1% KOH. Bone was then stained with a 0.005% Alizarin red solution for 4 h. Specimens were stored in a 50% glycerol-50% (1%) KOH solution until completely cleared. Images were acquired using a Leica Microsystems S9I Stereomicroscope and were processed using Adobe Photoshop software (CS6).

Single-cell RNA-sequencing—Control (*SOXC^{WT}*) and mutant (*SOXC^{Prx1Cre}*) littermates were collected at five developmental stages. At E11.5 to E15.5, their entire cranial mesenchyme was dissected and used for sequencing. At E17.5, only calvarial bones and connected tissues (periosteum, hypodermis and dura mater) were collected. Cranial

tissues were digested with Liberase™ (1 mg/mL in PBS) for 10 min (E11.5-E13.5) or 30 min (E15.5 and E17.5) at 37°C. Single cells were then passed through a 40 µm strainer, counted with a hemocytometer, and encapsulated into emulsion droplets using 10X Genomics Chromium Controller. Libraries were constructed for scRNA-seq using Chromium Single Cell 3' v2 or v3 Reagent Kit according to the manufacturer's protocol and were sequenced on a Illumina NovaSeq sequencer. Data were processed using the 10X Genomics workflow. In brief, Cell Ranger was used for demultiplexing, barcode assignment and unique molecular identifier (UMI) quantification. Downstream analyses were performed using Seurat v3, Monocle 3 and velocity. Cells with >6000 expressed genes, <200 expressed genes, or >20% mitochondrial transcripts were excluded. Data were normalized and integrated as described (Stuart et al., 2019). Next, cell cycle effects were regressed out whenever indicated, and Principal Component Analysis and Uniform Manifold Approximation and Projection (UMAP) were performed. Osteodermal lineage cells were subjected to trajectory modeling and pseudotemporal ordering in Monocle 3 (Cao et al., 2019). Spliced and unspliced reads were annotated using velocity.py as described (La Manno et al., 2018). Annotations were then transferred to the relative Seurat object and RNA velocity was estimated using velocity.R.

Differential gene expression analyses—Genes expressed differentially among cell clusters were identified using the Seurat FindMarkers function, applying a logarithmic fold change threshold 0.25. Significantly down- and upregulated genes (p value 0.05) were hierarchically clustered using dist and hclust functions in R. Genes with similar temporal expression patterns in control cells were grouped together. Gene Ontology (GO) analyses for enriched biological processes were performed on lists of differentially expressed genes using enrichGO function in clusterProfiler package (Wu et al., 2021). Output data were considered statistically significant for p values 0.05 after false discovery rate correction using Benjamini–Hochberg procedure.

Histology analysis and *in situ* assays—For Goldner's Trichrome staining, RISH and immunostaining assays, mouse heads were fixed in 4% paraformaldehyde for 24 h. E17.5-P0 specimens were then demineralized in Morse's or 15% EDTA solution for 24 h. Paraffin and frozen sections were made at 7-µm thickness in the coronal plane. Goldner's Trichrome staining was performed on paraffin sections. Briefly, sections deparaffinized were sequentially stained with Weigert's Hematoxylin (10 min), Ponceau Acid Fuchsin (5 min), Phosphomolybdic Acid-Orange G (10 min) and Light Green (5 min) solutions, and mounted using VectaMount Mounting Medium). RISH was performed using RNA-scope 2.5 HD detection reagent kit-RED on paraffin sections, as described (de Charleroy et al., 2021). Probes are listed in Table S4. Cell proliferation was assessed by Click-iT® EdU Alexa Fluor® 488 Imaging Kit, as described (Angelozzi et al., 2021). EdU (5-ethynyl-2'-deoxyuridine) was injected intraperitoneally in pregnant dams at 250 µg/10 g body weight 30 min before euthanasia. Cell death was assessed using the ApopTag Fluorescein In Situ Apoptosis Detection kit following manufacturer's instructions. Phospho-histone H3 (pH3) staining was performed on paraffin sections using a polyclonal anti-pH3 (Ser10) antibody (dilution 1:100), after antigen retrieval in citrate buffer, pH 6.0 for 2 h at 60°C and incubation in blocking buffer (TBS-T 0.1% with 10% serum) for 30

min at room temperature. Positive signals were detected with a biotinylated secondary anti-rabbit antibody (dilution 1:500) and amplified with a TSA-Fluorescein kit. Slides were counterstained with DAPI and mounted using ProLong™ Gold Antifade Mountant. Tomato fluorescent protein was detected in frozen sections after counterstaining with DAPI. Images were acquired using a Leica TCS SP8 confocal microscope or ZEISS Axio Scan.Z1 slide scanner microscope, and were processed using AdobePhotoshop (CS6). For RNA *in situ* hybridization assays, the blue color generated by hematoxylin counterstaining was desaturated (changed to grey) in all pictures by AdobePhotoshop. EdU- and pH3-positive cells were counted using ImageJ.

Supplementary Material

Refer to Web version on PubMed Central for supplementary material.

ACKNOWLEDGMENTS

We thank Pallavi Bhattaram, James Garifallou, Fernanda Mafra Thompson, and Charles de Charleroy for scientific advice and technical assistance. This work was supported by the National Institute of Arthritis and Musculoskeletal and Skin Diseases R01 grant AR068308, to V.L.

REFERENCES

- Aldeiri B, Roostalu U, Albertini A, Wong J, Morabito A, and Cossu G (2017). Transgelin-expressing myofibroblasts orchestrate ventral midline closure through TGFβ signalling. *Development* 144, 3336–3348. 10.1242/dev.152843. [PubMed: 28807903]
- Angelozzi M, de Charleroy CR, and Lefebvre V (2021). EdU-based assay of cell proliferation and stem cell quiescence in skeletal tissue sections. *Methods Mol. Biol* 2230, 357–365. 10.1007/978-1-0716-1028-2_21. [PubMed: 33197025]
- Angelozzi M, Karvande A, Molin AN, Ritter AL, Leonard JMM, Savatt JM, Douglass K, Myers SM, Grippa M, Tolchin D, et al. (2022). Consolidation of the clinical and genetic definition of a SOX4-related neurodevelopmental syndrome. *J. Med. Genet* 10.1136/jmedgenet-2021-108375.
- Angelozzi M, and Lefebvre V (2019). SOXopathies: growing family of developmental disorders due to SOX mutations. *Trends Genet.* 35, 658–671. 10.1016/j.tig.2019.06.003. [PubMed: 31288943]
- Bhattaram P, Muschler G, Wixler V, and Lefebvre V (2018). Inflammatory cytokines stabilize SOXC transcription factors to mediate the transformation of fibroblast-like synoviocytes in arthritic disease. *Arthritis Rheumatol.* 70, 371–382. 10.1002/art.40386. [PubMed: 29193895]
- Bhattaram P, Penzo-Méndez A, Kato K, Bandyopadhyay K, Gadi A, Taketo MM, and Lefebvre V (2014). SOXC proteins amplify canonical WNT signaling to secure nonchondrocytic fates in skeletogenesis. *J. Cell Biol* 207, 657–671. 10.1083/jcb.201405098. [PubMed: 25452386]
- Bhattaram P, Penzo-Méndez A, Sock E, Colmenares C, Kaneko KJ, Vassilev A, Depamphilis ML, Wegner M, and Lefebvre V (2010). Organogenesis relies on SoxC transcription factors for the survival of neural and mesenchymal progenitors. *Nat. Commun* 1, 9. 10.1038/ncomms1008. [PubMed: 20596238]
- Canalis E, Smerdel-Ramoya A, Durant D, Economides AN, Beamer WG, and Zanotti S (2010). Nephroblastoma overexpressed (Nov) inactivation sensitizes osteoblasts to bone morphogenetic protein-2, but nov is dispensable for skeletal homeostasis. *Endocrinology* 151, 221–233. 10.1210/en.2009-0574. [PubMed: 19934377]
- Cao J, Spielmann M, Qiu X, Huang X, Ibrahim DM, Hill AJ, Zhang F, Mundlos S, Christiansen L, Steemers FJ, et al. (2019). The single-cell transcriptional landscape of mammalian organogenesis. *Nature* 566, 496–502. 10.1038/s41586-019-0969-x. [PubMed: 30787437]
- Cunnington RH, Northcott JM, Ghavami S, Filomeno KL, Jahan F, Kavosh MS, Davies JLL, Wigle JT, and Dixon IMC (2014). The Ski-Zeb2-Meox2 pathway provides a novel mechanism for regulation

of the cardiac myofibroblast phenotype. *J. Cell Sci* 127, 40–49. 10.1242/jcs.126722. [PubMed: 24155330]

Dasgupta K, Chung JU, Asam K, and Jeong J (2019). Molecular patterning of the embryonic cranial mesenchyme revealed by genome-wide transcriptional profiling. *Dev. Biol* 455, 434–448. 10.1016/j.ydbio.2019.07.015. [PubMed: 31351040]

Dasgupta K, and Jeong J (2019). Developmental biology of the meninges. *Genesis* 57, e23288. 10.1002/dvg.23288. [PubMed: 30801905]

de Charleroy C, Haseeb A, and Lefebvre V (2021). Preparation of adult mouse skeletal tissue sections for RNA in situ hybridization. *Methods Mol. Biol* 2245, 85–92. 10.1007/978-1-0716-1119-7_6. [PubMed: 33315196]

DeSisto J, O'Rourke R, Jones HE, Pawlikowski B, Malek AD, Bonney S, Guimiot F, Jones KL, and Siegenthaler JA (2020). Single-cell transcriptomic analyses of the developing meninges reveal meningeal fibroblast diversity and function. *Dev. Cell* 54, 43–59.e4. 10.1016/j.devcel.2020.06.009. [PubMed: 32634398]

Driskell RR, Lichtenberger BM, Hoste E, Kretzschmar K, Simons BD, Charalambous M, Ferron SR, Haurault Y, Pavlovic G, Ferguson-Smith AC, and Watt FM (2013). Distinct fibroblast lineages determine dermal architecture in skin development and repair. *Nature* 504, 277–281. 10.1038/nature12783. [PubMed: 24336287]

Dy P, Penzo-Méndez A, Wang H, Pedraza CE, Macklin WB, and Lefebvre V (2008). The three SoxC proteins—Sox4, Sox11 and Sox12—exhibit overlapping expression patterns and molecular properties. *Nucleic Acids Res.* 36, 3101–3117. 10.1093/nar/gkn162. [PubMed: 18403418]

Farmer DT, Mlcochova H, Zhou Y, Koelling N, Wang G, Ashley N, Bugacov H, Chen HJ, Parvez R, Tseng KC, et al. (2021). The developing mouse coronal suture at single-cell resolution. *Nat. Commun* 12, 4797. 10.1038/s41467-021-24917-9. [PubMed: 34376651]

Foronda M, Morgado-Palacin L, Gómez-López G, Domínguez O, Pisano DG, and Blasco MA (2015). Profiling of Sox4-dependent transcriptome in skin links tumour suppression and adult stem cell activation. *Genom Data* 6, 21–24. 10.1016/j.gdata.2015.07.030. [PubMed: 26697322]

Gadi J, Jung SH, Lee MJ, Jami A, Ruthala K, Kim KM, Cho NH, Jung HS, Kim CH, and Lim SK (2013). The transcription factor protein Sox11 enhances early osteoblast differentiation by facilitating proliferation and the survival of mesenchymal and osteoblast progenitors. *J. Biol. Chem* 288, 25400–25413. 10.1074/jbc.m112.413377. [PubMed: 23888050]

Goodnough LH, Dinuoscio GJ, and Atit RP (2016). Twist1 contributes to cranial bone initiation and dermal condensation by maintaining Wnt signaling responsiveness. *Dev. Dynam* 245, 144–156. 10.1002/dvdy.24367.

Holmes G, Gonzalez-Reiche AS, Lu N, Zhou X, Rivera J, Kriti D, Sebra R, Williams AA, Donovan MJ, Potter SS, et al. (2020). Integrated transcriptome and network analysis reveals spatiotemporal dynamics of calvarial suturogenesis. *Cell Rep.* 32, 107871. 10.1016/j.celrep.2020.107871. [PubMed: 32640236]

Hoser M, Potzner MR, Koch JMC, Bosl MR, Wegner M, and Sock E (2008). Sox12 deletion in the mouse reveals nonreciprocal redundancy with the related Sox4 and Sox11 transcription factors. *Mol. Cell Biol* 28, 4675–4687. 10.1128/mcb.00338-08. [PubMed: 18505825]

Huang H, Yang X, Bao M, Cao H, Miao X, Zhang X, Gan L, Qiu M, and Zhang Z (2016). Ablation of the Sox11 gene results in clefting of the secondary palate resembling the pierre robin sequence. *J. Biol. Chem* 291, 7107–7118. 10.1074/jbc.m115.690875. [PubMed: 26826126]

Huang W, and Olsen BR (2015). Skeletal defects in Osterix-Cre transgenic mice. *Transgenic Res.* 24, 167–172. 10.1007/s11248-014-9828-6. [PubMed: 25139670]

Ishii M, Sun J, Ting MC, and Maxson RE (2015). The development of the calvarial bones and sutures and the pathophysiology of craniosynostosis. *Curr. Top. Dev. Biol* 115, 131–156. 10.1016/bs.ctdb.2015.07.004. [PubMed: 26589924]

Jiang X, Iseki S, Maxson RE, Sucov HM, and Morriss-Kay GM (2002). Tissue origins and interactions in the mammalian skull vault. *Dev. Biol* 241, 106–116. 10.1006/dbio.2001.0487. [PubMed: 11784098]

Kamachi Y, and Kondoh H (2013). Sox proteins: regulators of cell fate specification and differentiation. *Development* 140, 4129–4144. 10.1242/dev.091793. [PubMed: 24086078]

- Kato K, Bhattaram P, Penzo-Méndez A, Gadi A, and Lefebvre V (2015). SOXC transcription factors induce cartilage growth plate formation in mouse embryos by promoting noncanonical WNT signaling. *J. Bone Miner. Res* 30, 1560–1571. 10.1002/jbmr.2504. [PubMed: 25761772]
- Kosaras B, Jakubowski M, Kainz V, and Burstein R (2009). Sensory innervation of the calvarial bones of the mouse. *J. Comp. Neurol* 515, 331–348. 10.1002/cne.22049. [PubMed: 19425099]
- La Manno G, Soldatov R, Zeisel A, Braun E, Hochgerner H, Petukhov V, Lidschreiber K, Kastri ME, Lönnberg P, Furlan A, et al. (2018). RNA velocity of single cells. *Nature* 560, 494–498. 10.1038/s41586-018-0414-6. [PubMed: 30089906]
- Lattanzi W, Barba M, Di Pietro L, and Boyadjiev SA (2017). Genetic advances in craniosynostosis. *Am. J. Med. Genet* 173, 1406–1429. 10.1002/ajmg.a.38159. [PubMed: 28160402]
- Logan M, Martin JF, Nagy A, Lobe C, Olson EN, and Tabin CJ (2002). Expression of Cre Recombinase in the developing mouse limb bud driven by a Prxl enhancer. *Genesis* 33, 77–80. 10.1002/gene.10092. [PubMed: 12112875]
- Madisen L, Zwingman TA, Sunkin SM, Oh SW, Zariwala HA, Gu H, Ng LL, Palmiter RD, Hawrylycz MJ, Jones AR, et al. (2010). A robust and high-throughput Cre reporting and characterization system for the whole mouse brain. *Nat. Neurosci* 13, 133–140. 10.1038/nn.2467. [PubMed: 20023653]
- Matsushita Y, Sakamoto K, Tamamura Y, Shibata Y, Minamizato T, Kihara T, Ito M, Katsube K.i., Hiraoka S, Koseki H, et al. (2013). CCN3 protein participates in bone regeneration as an inhibitory factor. *J. Biol. Chem* 288, 19973–19985. 10.1074/jbc.m113.454652. [PubMed: 23653360]
- Miao Q, Hill MC, Chen F, Mo Q, Ku AT, Ramos C, Sock E, Lefebvre V, and Nguyen H (2019). SOX11 and SOX4 drive the reactivation of an embryonic gene program during murine wound repair. *Nat. Commun* 10, 4042. 10.1038/s41467-019-11880-9. [PubMed: 31492871]
- Moreno CS (2020). SOX4: the unappreciated oncogene. *Semin. Cancer Biol* 67, 57–64. 10.1016/j.semcancer.2019.08.027. [PubMed: 31445218]
- Morriss-Kay GM, and Wilkie AOM (2005). Growth of the normal skull vault and its alteration in craniosynostosis: insights from human genetics and experimental studies. *J. Anat* 207, 637–653. 10.1111/j.1469-7580.2005.00475.x. [PubMed: 16313397]
- Mundlos S, Otto F, Mundlos C, Mulliken JB, Aylsworth AS, Albright S, Lindhout D, Cole WG, Henn W, Knoll JH, et al. (1997). Mutations involving the transcription factor CBFA1 cause cleidocranial dysplasia. *Cell* 89, 773–779. 10.1016/s0092-8674(00)80260-3. [PubMed: 9182765]
- Nissen-Meyer LSH, Jemtland R, Gautvik VT, Pedersen ME, Paro R, Fortunati D, Pierroz DD, Stadelmann VA, Reppe S, Reinholt FP, et al. (2007). Osteopenia, decreased bone formation and impaired osteoblast development in Sox4 heterozygous mice. *J. Cell Sci* 120, 2785–2795. 10.1242/jcs.003855. [PubMed: 17652162]
- Pakshir P, Noskovicova N, Lodyga M, Son DO, Schuster R, Goodwin A, Karvonen H, and Hinz B (2020). The myofibroblast at a glance. *J. Cell Sci* 133, jcs227900. 10.1242/jcs.227900. [PubMed: 32651236]
- Paul MH, Harvey RP, Wegner M, and Sock E (2014). Cardiac outflow tract development relies on the complex function of Sox4 and Sox11 in multiple cell types. *Cell. Mol. Life Sci* 71, 2931–2945. 10.1007/s00018-013-1523-x. [PubMed: 24310815]
- Penzo-Méndez A, Dy P, Pallavi B, and Lefebvre V (2007). Generation of mice harboring a Sox4 conditional null allele. *Genesis* 45, 776–780. 10.1002/dvg.20358. [PubMed: 18064674]
- R Core Team (2020). R: A Language and Environment for Statistical Computing (Vienna, Austria: R Foundation for Statistical Computing).
- Richtsmeier JT, and Flaherty K (2013). Hand in glove: brain and skull in development and dysmorphogenesis. *Acta Neuropathol.* 125, 469–489. 10.1007/s00401-013-1104-y. [PubMed: 23525521]
- Rigueur D, and Lyons KM (2014). Whole-mount skeletal staining. *Methods Mol. Biol* 1130, 113–121. 10.1007/978-1-62703-989-5_9. [PubMed: 24482169]
- Rodda SJ, and McMahon AP (2006). Distinct roles for Hedgehog and canonical Wnt signaling in specification, differentiation and maintenance of osteoblast progenitors. *Development* 133, 3231–3244. 10.1242/dev.02480. [PubMed: 16854976]
- RStudio Team (2020). RStudio: Integrated Development for R (RStudio, PBC).

- Schilham MW, Oosterwegel MA, Moerer P, Ya J, de Boer PAJ, van de Wetering M, Verbeek S, Lamers WH, Kruisbeek AM, Cumano A, and Clevers H (1996). Defects in cardiac outflow tract formation and pro-B-lymphocyte expansion in mice lacking Sox-4. *Nature* 380, 711–714. 10.1038/380711a0. [PubMed: 8614465]
- Schneider CA, Rasband WS, and Eliceiri KW (2012). NIH Image to ImageJ: 25 years of image analysis. *Nat. Methods* 9, 671–675. 10.1038/nmeth.2089. [PubMed: 22930834]
- Sennett R, Wang Z, Rezza A, Grisanti L, Roitershtein N, Sicchio C, Mok KW, Heitman NJ, Clavel C, Ma'ayan A, and Rendl M (2015). An integrated transcriptome atlas of embryonic hair follicle progenitors, their niche, and the developing skin. *Dev. Cell* 34, 577–591. 10.1016/j.devcel.2015.06.023. [PubMed: 26256211]
- Seo HS, and Serra R (2009). Tgfr2 is required for development of the skull vault. *Dev. Biol* 334, 481–490. 10.1016/j.ydbio.2009.08.015. [PubMed: 19699732]
- Sharma AK, Kothari SK, Agarwal LD, and Sharma A (2001). Agenesis of the skull bones. *Pediatr. Surg. Int* 17, 452–454. 10.1007/s003830000511. [PubMed: 11527187]
- Sock E, Rettig SD, Enderich J, Bosl MR, Tamm ER, and Wegner M (2004). Gene targeting reveals a widespread role for the high-mobility-group transcription factor Sox11 in tissue remodeling. *Mol. Cell Biol* 24, 6635–6644. 10.1128/mcb.24.15.6635-6644.2004. [PubMed: 15254231]
- Stuart T, Butler A, Hoffman P, Hafemeister C, Papalexi E, Mauck WM 3rd, Hao Y, Stoeckius M, Smibert P, and Satija R (2019). Comprehensive integration of single-cell dData. *Cell* 177, 1888–1902.e1821. [PubMed: 31178118]
- Svitkina T (2018). The Actin Cytoskeleton and actin-based motility. *Cold Spring Harbor Perspect. Biol* 10, a018267. 10.1101/cshperspect.a018267.
- Takarada T, Nakazato R, Tsuchikane A, Fujikawa K, Iezaki T, Yoneda Y, and Hinoi E (2016). Genetic analysis of Runx2 function during intramembranous ossification. *Development* 143, 211–218. 10.1242/dev.128793. [PubMed: 26657773]
- Timberlake AT, Jin SC, Nelson-Williams C, Wu R, Furey CG, Islam B, Haider S, Loring E, Galm A, Steinbacher DM, et al. (2019). Mutations in TFAP2B and previously unimplicated genes of the BMP, Wnt, and Hedgehog pathways in syndromic craniosynostosis. *Proc. Natl. Acad. Sci. USA* 116, 15116–15121. 10.1073/pnas.1902041116. [PubMed: 31292255]
- Ting MC, Wu NL, Roybal PG, Sun J, Liu L, Yen Y, and Maxson RE Jr. (2009). EphA4 as an effector of Twist1 in the guidance of osteogenic precursor cells during calvarial bone growth and in craniosynostosis. *Development* 136, 855–864. 10.1242/dev.028605. [PubMed: 19201948]
- Tiwari N, Tiwari VK, Waldmeier L, Balwierz PJ, Arnold P, Pachkov M, Meyer-Schaller N, Schübeler D, Schubeler D, van Nimwegen E, and Christofori G (2013). Sox4 is a master regulator of epithelial-mesenchymal transition by controlling Ezh2 expression and epigenetic reprogramming. *Cancer Cell* 23, 768–783. 10.1016/j.ccr.2013.04.020. [PubMed: 23764001]
- Tran TH, Jarrell A, Zentner GE, Welsh A, Brownell I, Scacheri PC, and Atit R (2010). Role of canonical Wnt signaling/ β -catenin via *Dermo1* in cranial dermal cell development. *Development* 137, 3973–3984. 10.1242/dev.056473. [PubMed: 20980404]
- Tsang SM, Oliemuller E, and Howard BA (2020). Regulatory roles for SOX11 in development, stem cells and cancer. *Semin. Cancer Biol* 67, 3–11. 10.1016/j.semcancer.2020.06.015. [PubMed: 32574812]
- Tsurusaki Y, Koshimizu E, Ohashi H, Phadke S, Kou I, Shiina M, Suzuki T, Okamoto N, Imamura S, Yamashita M, et al. (2014). De novo SOX11 mutations cause Coffin-Siris syndrome. *Nat. Commun* 5, 4011. 10.1038/ncomms5011. [PubMed: 24886874]
- Tubbs RS, Bosmia AN, and Cohen-Gadol AA (2012). The human calvaria: a review of embryology, anatomy, pathology, and molecular development. *Childs Nerv Syst* 28, 23–31. 10.1007/s00381-011-1637-0. [PubMed: 22120469]
- Vasudevan HN, and Soriano P (2014). SRF regulates craniofacial development through selective recruitment of MRTF cofactors by PDGF signaling. *Dev. Cell* 31, 332–344. 10.1016/j.devcel.2014.10.005. [PubMed: 25453829]
- Wang L, Hou S, Sabsovich I, Guo TZ, Wei T, and Kingery WS (2021). Mice lacking substance P have normal bone modeling but diminished bone formation, increased resorption, and accelerated osteopenia with aging. *Bone* 144, 115806. 10.1016/j.bone.2020.115806. [PubMed: 33333245]

- Wang L, Mishina Y, and Liu F (2015). Osterix-Cre transgene causes craniofacial bone development defect. *Calcif. Tissue Int* 96, 129–137. 10.1007/s00223-014-9945-5. [PubMed: 25550101]
- Wickham H (2016). *ggplot2: Elegant Graphics for Data Analysis* (New York: Springer-Verlag).
- Wu T, Hu E, Xu S, Chen M, Guo P, Dai Z, Feng T, Zhou L, Tang W, Zhan L, et al. (2021). clusterProfiler 4.0: a universal enrichment tool for interpreting omics data. *Innovation* 2, 100141. 10.1016/j.xinn.2021.100141. [PubMed: 34557778]
- Yoshida GJ (2020). Regulation of heterogeneous cancer-associated fibroblasts: the molecular pathology of activated signaling pathways. *J. Exp. Clin. Cancer Res* 39, 112. 10.1186/s13046-020-01611-0. [PubMed: 32546182]
- Yu F, Wu F, Li F, Liao X, Wang Y, Li X, Wang C, Shi Y, and Ye L (2020). Wnt7b-induced Sox11 functions enhance self-renewal and osteogenic commitment of bone marrow mesenchymal stem cells. *Stem Cell.* 38, 1020–1033. 10.1002/stem.3192.
- Zawerton A, Yao B, Yeager JP, Pippucci T, Haseeb A, Smith JD, Wischmann L, Kühl SJ, Dean JCS, Pilz DT, et al. (2019). De novo SOX4 variants cause a neurodevelopmental disease associated with mild dysmorphism. *Am. J. Hum. Genet* 104, 246–259. 10.1016/j.ajhg.2018.12.014. [PubMed: 30661772]

Highlights

- Single-cell transcriptomics at five embryo stages shed light on craniogenesis
- Cranial cells include intermediate progenitors with a myofibroblast-like signature
- SOXC deletion in early progenitors impairs cranial bone and dermis development
- SOXC foster progenitors' myofibroblastic traits and proliferation, not lineage fate

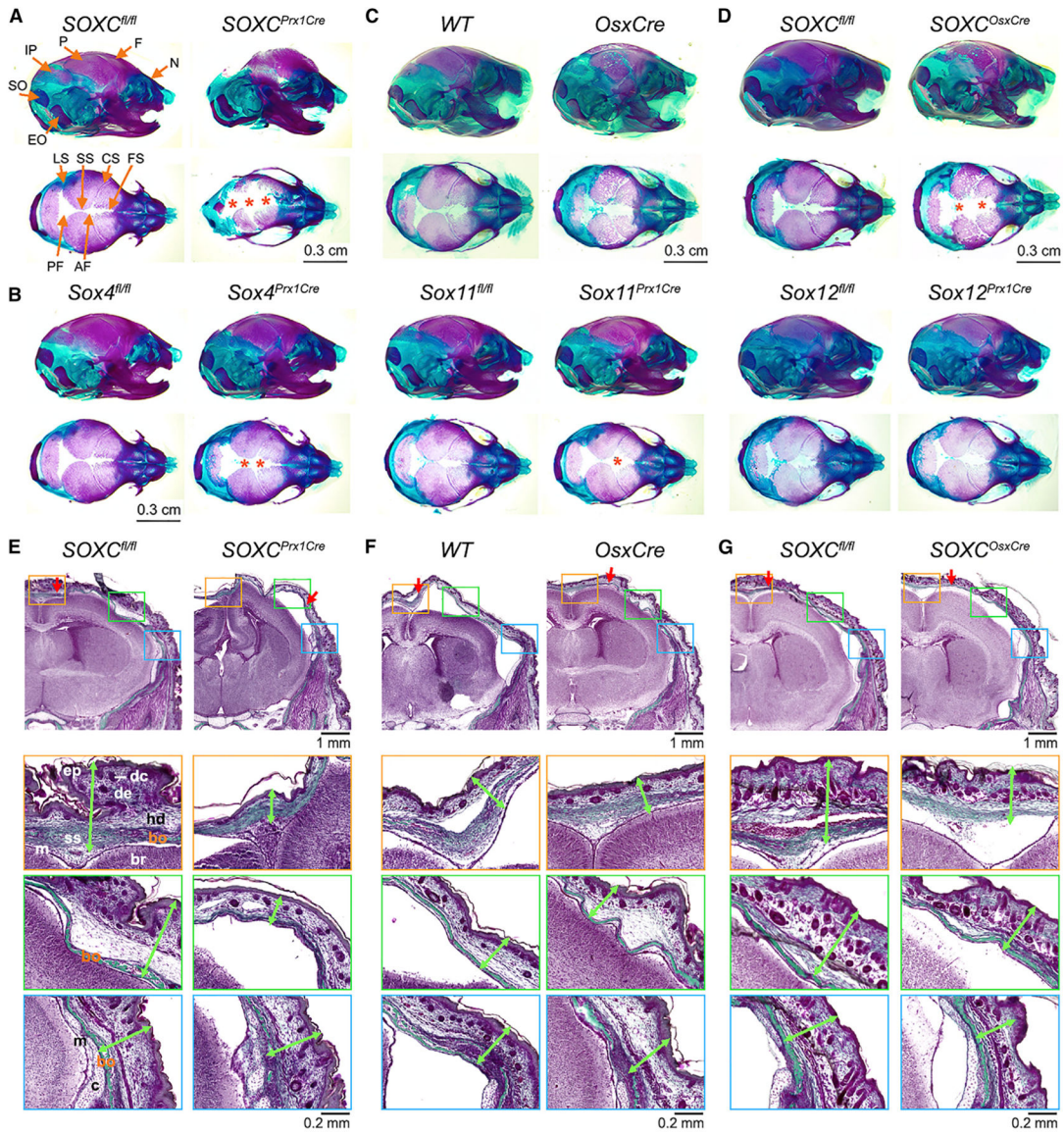


Figure 1. SOXC are necessary for proper craniogenesis

(A) Skeletal preparations of E18.5 control and *SOXC^{Prx1Cre}* littermate heads. Bone is stained with alizarin red and cartilage with Alcian blue. Asterisks, bone defects. EO, exoccipital; SO, supraoccipital; IP, interparietal; P, parietal; F, frontal; and N, nasal bones. LS, lambdoid; SS, sagittal; CS, coronal; and FS, frontal sutures. PF, posterior; and AF, anterior fontanelles.

(B) Skeletal preparations of E18.5 control and single *SOXC^{Prx1Cre}* littermate heads.

(C) Skeletal preparations of newborn (P0) control and *OsxCre* littermate heads. Note the fenestration of *OsxCre* bones.

(D) Skeletal preparations of P0 control and *SOXC^{OsxCre}* littermate heads. Note that bone apex defects are milder in *SOXC^{OsxCre}* than *SOXC^{Prx1Cre}* heads.

(E) Masson-Goldner trichrome staining of coronal sections through parietal bones of E18.5 control and *SOXC^{Prx1Cre}* littermates. Top row, low-magnification images. Other rows,

enlarged pictures of regions boxed in top row. Bo, bone; br, brain; C, temporal bone cartilage primordium; dc, dermal condensate; De, dermis; Ep, epidermis; Hd, hypodermis; M, meninges; Ss, sagittal suture. Red arrows, apical tip of mineralized bone. Green double arrows, cranium depth.

(F) Same analysis as in (C), but for P0 control and *OsxCre* littermates. Note that *OsxCre* delayed bone mineralization at the apex.

(G) Same analysis as in (C), but for P0 control and *SOXC^{OsxCre}* littermates. See Figure S2 for complementary data.

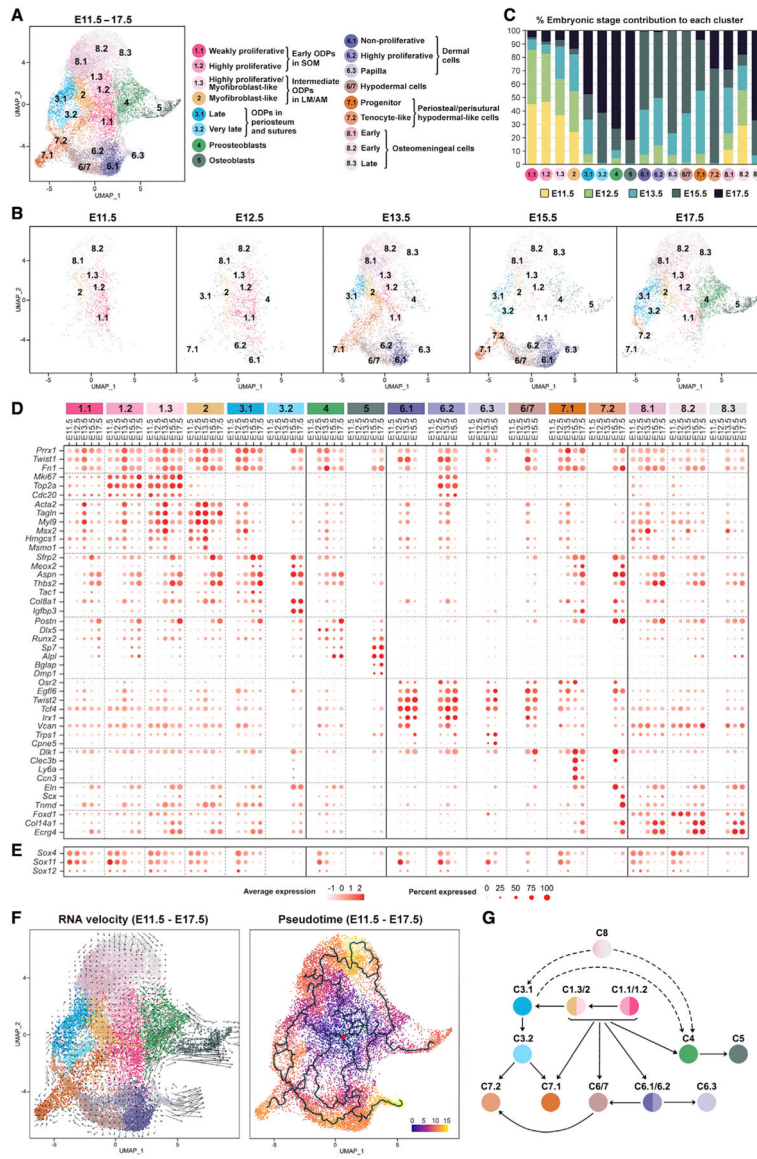


Figure 2. Transcriptome profiling identifies distinct osteo/dermal populations in E11.5 to E17.5 crania
 (A) UMAP plot of osteo/dermal clusters obtained by re-clustering the E11.5–E17.5 C1–C8 clusters of *Prrx1^{med/high}* cells shown in Figure S3F. Clusters are numbered based on parental clusters and named based on marker expression (see D) and spatial location (see Figure 3).
 (B) UMAP plots of the same populations as in (A), but at individual developmental stages.
 (C) Percentages of cells from each developmental stage that contribute to cluster formation.
 (D) Dot plot showing expression of markers used to identify clusters. Dot color intensity reflects average gene expression per cell, and dot size reflects percentage of gene-expressing cells. Data for clusters with <20 cells are not reported. No data were obtained for E17.5 C6.1–C6/7 cells.
 (E) Dot plot of SOXC expression.
 (F) RNA velocity and pseudotime analyses of E11.5–E17.5 osteo/dermal cells. The red dot in the pseudotime graph shows the initial root.
 (G) Lineage diagram showing cell clusters and their relationships.

(G) Schematic of predicted cluster relationships. Full lines, major links. Dotted lines, minor links.

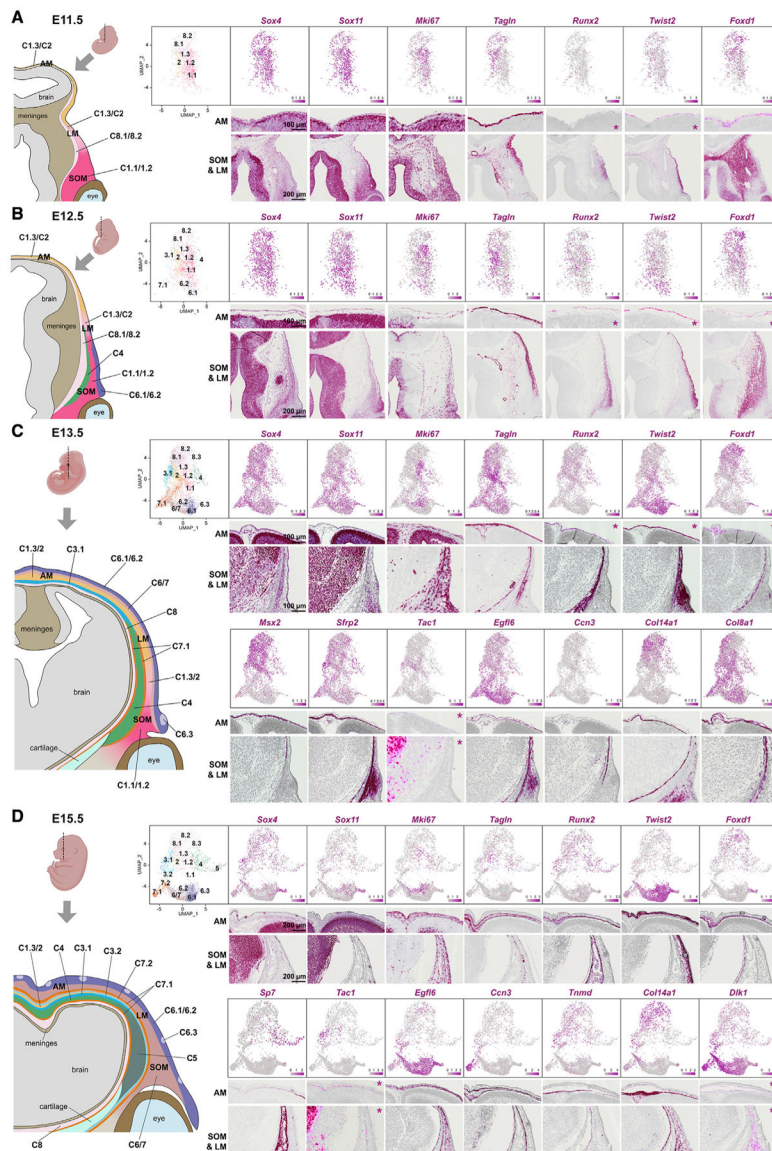


Figure 3. RISH spatially maps cranial cell populations identified by scRNA-seq
 (A) Top right, UMAP plots showing E11.5 osteo/dermal cranial populations and expression of markers. Bottom right, RISH on coronal sections at the level of the SOM and presumptive parietal bone and sagittal suture. Asterisks mark the images in which RISH signals were amplified by saturating the magenta color using Adobe Photoshop. Left, schematic of an equivalent section mapping cranial populations.
 (B–D) Similar data and presentations as in (A), but for later stage samples.
 See Figure S4 for pictures of RISH in the entire head regions depicted in the schematics. See Figure S5 for additional RISH at E15.5 and for data at E17.5.

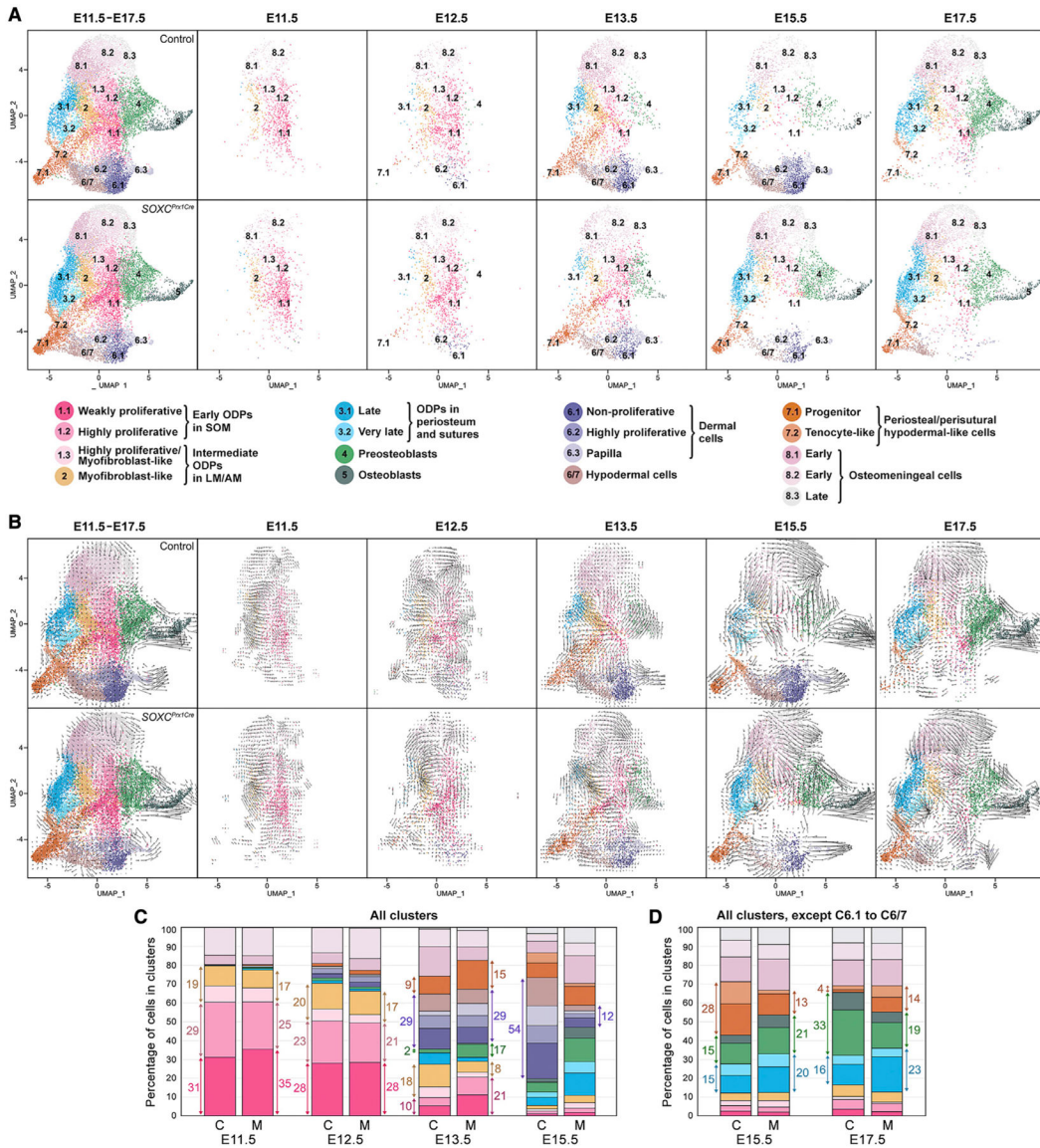


Figure 4. Cranial osteo/dermal clusters show differences between control and *SOXC^{Prx1Cre}* embryos

(A) UMAP plots of osteo/dermal clusters in *SOXC^{Prx1Cre}* and control embryos at all and individual developmental stages.

(B) RNA velocity analysis of the same samples as in (A). See pseudotime analyses in Figure S6A.

(C) Relative proportions of osteo/dermal clusters in control (C) and mutant (M) cranial populations at E11.5–E15.5. Double arrows indicate percentage values for selected clusters. Clusters are colored as in (A).

(D) Same representation as in (C), but after exclusion of C6.1–C6/7 in E15.5 and E17.5 samples.

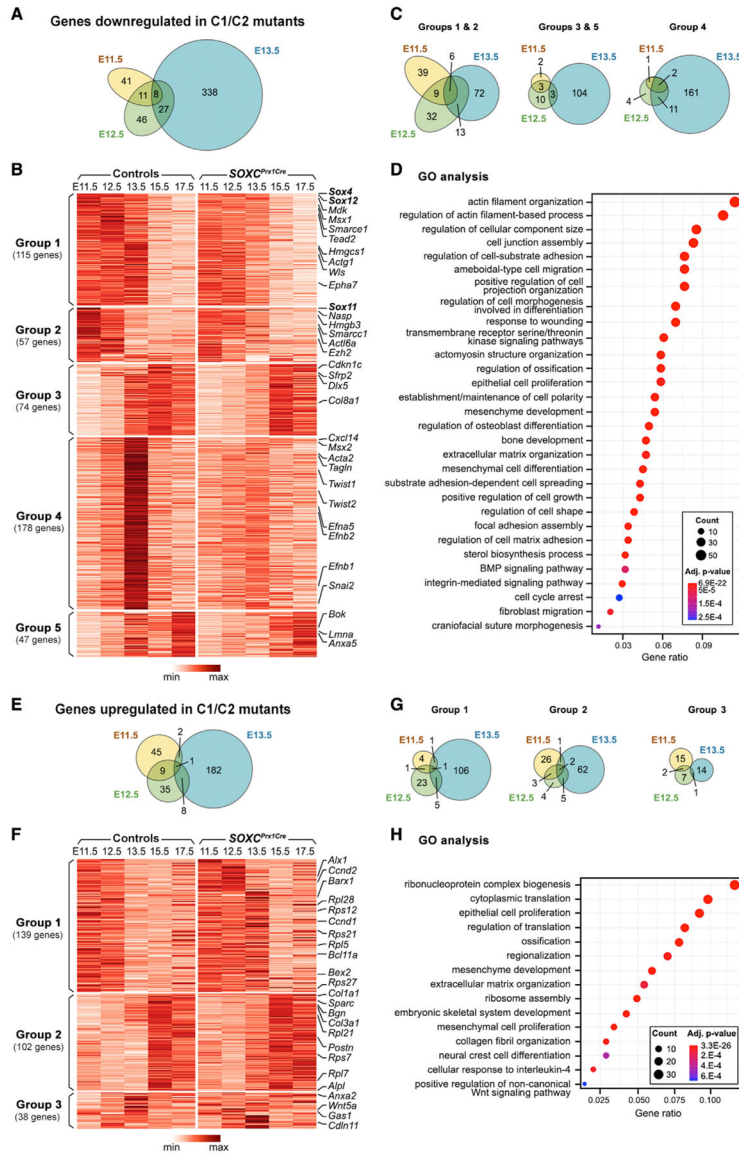


Figure 5. Global analysis reveals transcriptome changes in *SOXC^{Prx1Cre}* ODPs
 (A) Venn diagrams showing the numbers of genes downregulated in E11.5–E13.5 mutant C1/C2 (FC 1.28, p 0.05).
 (B) Heatmaps of the expression levels of downregulated genes. Genes fall into 5 groups according to temporal expression patterns in controls. A few genes of interest are marked.
 (C) Venn diagrams showing when genes in the 5 groups are downregulated in mutants.
 (D) GO analysis of all downregulated genes. See Figure S6B for analyses of selected groups.
 (E) Venn diagrams showing the numbers of genes upregulated in E11.5–E13.5 C1/C2 mutants (FC 1.28, p 0.05).
 (F) Heatmaps of the expression levels of upregulated genes. Genes fall into 3 groups according to temporal expression patterns in controls. A few genes of interest are identified.
 (G) Venn diagrams showing when genes in the 3 groups are upregulated in mutants.
 (H) GO analysis of all upregulated genes. See Figure S6C for analyses of selected groups.

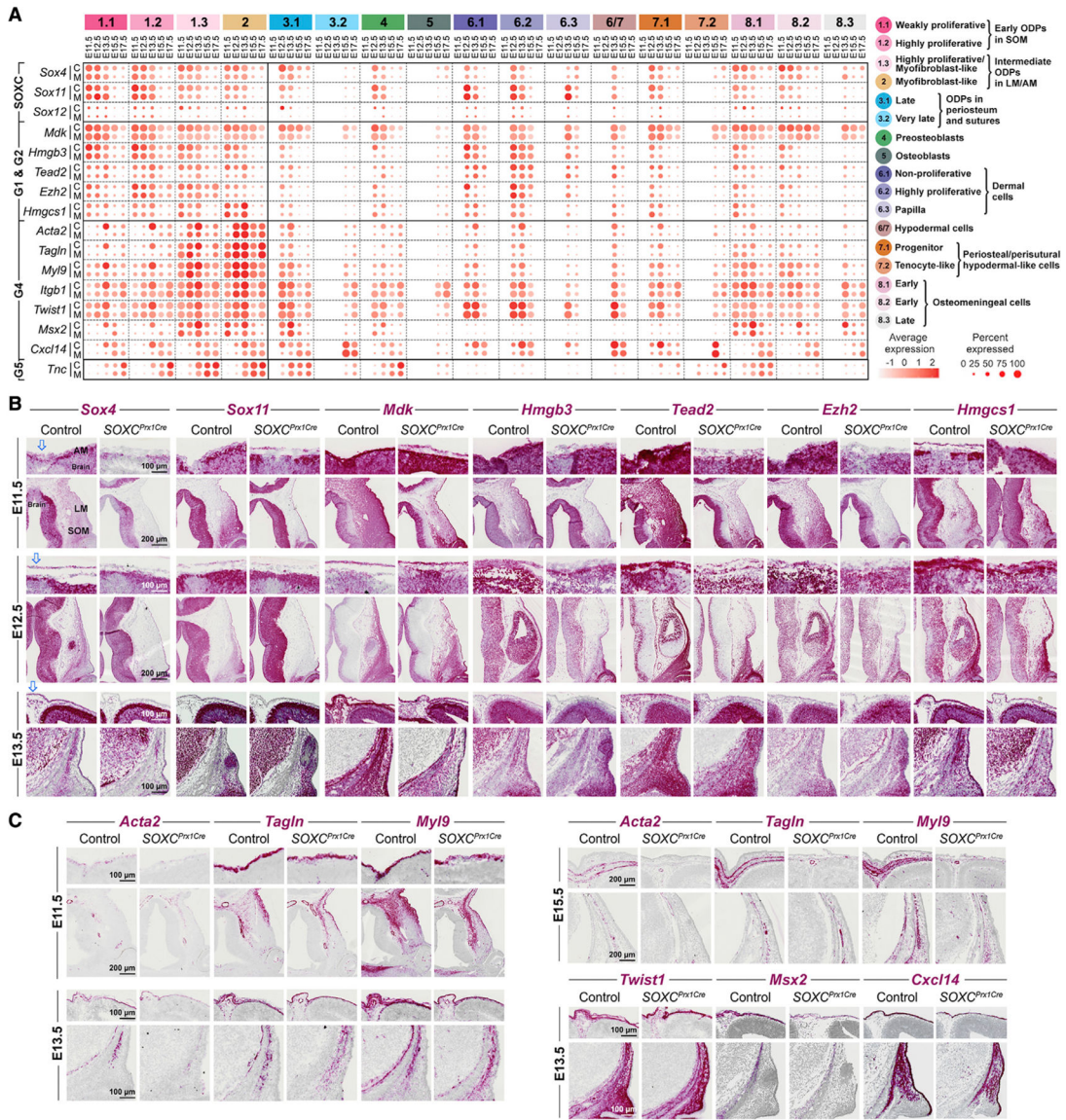


Figure 6. RISH validates downregulation of selected genes in *SOXC^{Prx1Cre}* ODPs

(A) Dot plot showing expression of SOXC and other genes downregulated in E11.5–E13.5. *SOXC^{Prx1Cre}* ODPs. Genes are presented in groups (G) as identified in Figure 5B. Data for clusters of <20 cells are not reported. No data were obtained for E17.5 C6.1–C6/7 cells. Of note, SOXC do not look fully inactivated in mutants, likely because null alleles lack the coding sequence (~1.5 kb), but still contain untranslated sequences (3–7 kb). C, control. M, mutant.

(B) RISH for *Sox4*, *Sox11* and other downregulated genes from groups 1 and 2. Coronal sections of E11.5–E13.5 embryo heads were analyzed at the level of the supraorbital mesenchyme and presumptive parietal bone. For each stage, the top row shows the apical mesenchyme (AM) region, and the bottom row shows the supraorbital (SOM) and lateral mesenchyme (LM) region. Descending arrow, medial line where the sagittal suture will later form.

(C) RISH at E11.5–E15.5 for group 4 downregulated genes. Data were generated and are presented as in (B). See Figure S7 for images of the entire sections.

Author Manuscript

Author Manuscript

Author Manuscript

Author Manuscript

mutant (M) littermate pairs per time point. p values from paired t tests are indicated. ns, not significant. See Figure S9 for complementary data.

Author Manuscript

Author Manuscript

Author Manuscript

Author Manuscript

KEY RESOURCES TABLE

REAGENT or RESOURCE	SOURCE	IDENTIFIER
Antibodies		
Rabbit polyclonal anti-pH3 (Ser10)	Cell Signaling Technology	Cat#9701S; RRID: AB_331535
Biotin-SP Donkey Anti-Rabbit IgG (H + L)	Jackson ImmunoResearch Laboratories, INC.	Cat# 711-065-152; RRID: AB_2340593
Chemicals, peptides, and recombinant proteins		
5-ethynyl-2'-deoxyuridine (EdU)	Thermo Fisher Scientific	Cat#A10044
Liberase™ TM Research Grade	Millipore Sigma	Cat#5401127001
4',6-Diamidino-2-Phenylindole, Dihydrochloride (DAPI)	Thermo Fisher Scientific	Cat#D1306
Custom pretreatment reagent	Advanced Cell Diagnostics	Cat#300040
O.C.T embedding medium	Fisher Scientific	Cat#23-730-571
Paraffin	Fisher Scientific	Cat#B1002490
Acid fuchsin	Millipore Sigma	Cat#F8129
Alcian Blue 8GX	Thermo Fisher Scientific	Cat#AC400460250
Alizarin Red S	Millipore Sigma	Cat#A5533
Gill's hematoxylin	Millipore Sigma	Cat#GHS132
Hematoxylin	Fisher Scientific	Cat#H345-25
Ponceau Xylidine	Millipore Sigma	Cat#P2395
Phosphomolybdic acid hydrate	Millipore Sigma	Cat#221856
Orange G	Fisher Scientific	Cat#O267-25
Light Green SF, Yellowish	Fisher Scientific	Cat#O3382-25
ProLong™ Gold Antifade Mountant	Thermo Fisher Scientific	Cat# P36930
VectaMount Mounting Medium	Vector Laboratories	Cat# H-5000-60
Critical commercial assays		
Click-iT™ EdU Cell Proliferation Kit for Imaging, Alexa Fluor™ 488 dye	Thermo Fisher Scientific	Cat#C10337
ApopTag® Plus In Situ Apoptosis Fluorescein Detection Kit	Millipore Sigma	Cat#S7111
TSA® Plus fluorescein detection kit	Akoya Biosciences	Cat#NEL741001KT
RNAscope® 2.5 HD Reagent Kit-RED	Advanced Cell Diagnostics	Cat#322350
Chromium Single Cell 3' Reagent Kit v2	10X Genomics	Cat#PN-120267
Chromium Single Cell 3' Reagent Kit v3	10X Genomics	Cat#PN-1000092
NovaSeq 6000 SP Reagent Kit v1.5 (100 cycles)	Illumina	Cat#20028401
Deposited data		
Single-cell RNA-seq data of control and SOXC-mutant crania	This paper	GEO: GSE174716
Experimental models: Organisms/strains		
Mouse: <i>Sox4</i> ^{fl/fl}	Dr. Véronique Lefebvre	Penzo-Mendez et al. (2007)
Mouse: <i>Sox11</i> ^{fl/fl}	Dr. Véronique Lefebvre	Bhattaram et al. (2010)
Mouse: <i>Sox12</i> ^{fl/fl}	Dr. Véronique Lefebvre	Bhattaram et al. (2010)
Mouse: <i>Prrx1</i> Cre; <i>B6.Cg-Tg(Prrx1-cre)1Cjt/J</i>	The Jackson Laboratory	JAX:005584

REAGENT or RESOURCE	SOURCE	IDENTIFIER
Mouse: <i>OsxCre; B6.Cg-Tg(Sp7-tTA,tetO-EGFP/cre)1Amc/J</i>	The Jackson Laboratory	JAX:006361
Mouse: <i>R26^{dT}; B6.Cg-Gt(ROSA)26Sortm14(CAG-tTomato)Hze/J</i>	The Jackson Laboratory	JAX:007914
Oligonucleotides		
ISH probe: Mm-Acta2	Advanced Cell Diagnostics	Cat#319531
ISH probe: Mm-Ccn3	Advanced Cell Diagnostics	Cat#415341
ISH probe: Mm-Col8a1	Advanced Cell Diagnostics	Cat#518071
ISH probe: Mm-Col14a1	Advanced Cell Diagnostics	Cat#581941
ISH probe: Mm-Dlk1	Advanced Cell Diagnostics	Cat#405971
ISH probe: Mm-Dmp1	Advanced Cell Diagnostics	Cat#441171
ISH probe: Mm-Foxd1	Advanced Cell Diagnostics	Cat#495501
ISH probe: Mm-Egfl6	Advanced Cell Diagnostics	Cat#316751
ISH probe: Mm-Ezh2	Advanced Cell Diagnostics	Cat#446611
ISH probe: Mm-Hmgb3	Advanced Cell Diagnostics	Cat#451381
ISH probe: Mm-Hmgcs1	Advanced Cell Diagnostics	Cat#556061
ISH probe: Mm-Mdk	Advanced Cell Diagnostics	Cat#537841
ISH probe: Mm-Mki67	Advanced Cell Diagnostics	Cat#416771
ISH probe: Mm-Msx2	Advanced Cell Diagnostics	Cat#421851
ISH probe: Mm-Myl9	Advanced Cell Diagnostics	Cat#480451
ISH probe: Mm-Runx2	Advanced Cell Diagnostics	Cat#414021
ISH probe: Mm-Sfrp2	Advanced Cell Diagnostics	Cat#400381
ISH probe: Mm-Sox4	Advanced Cell Diagnostics	Cat#471381
ISH probe: Mm-Sox11	Advanced Cell Diagnostics	Cat#440811
ISH probe: Mm-Sp7	Advanced Cell Diagnostics	Cat#403401
ISH probe: Mm-Tac1	Advanced Cell Diagnostics	Cat#410351
ISH probe: Mm-Tagln	Advanced Cell Diagnostics	Cat#480331
ISH probe: Mm-Tead2	Advanced Cell Diagnostics	Cat#420281
ISH probe: Mm-Tnmd	Advanced Cell Diagnostics	Cat#430531
ISH probe: Mm-Twist1	Advanced Cell Diagnostics	Cat#414701
ISH probe: Mm-Twist2	Advanced Cell Diagnostics	Cat#489121
Software and algorithms		
Cell Ranger	10X Genomics	https://support.10xgenomics.com/single-cell-gene-expression/software/overview/welcome
Seurat (version 4.1.0)	Stuart et al. (2019)	https://satijalab.org/seurat/
Velocyto	La Manno et al. (2018)	https://velocyto.org
Monocle 3	Cao et al. (2019)	https://cole-trapnell-lab.github.io/monocle3/
ImageJ	Schneider et al. (2012)	https://imagej.nih.gov/ij/
Adobe Photoshop (CS6)	Adobe Inc.	https://www.adobe.com/products/photoshop.html
clusterProfiler (version 3.18.1)	Wu et al. (2021)	https://bioconductor.org/packages/release/bioc/html/clusterProfiler.html
ggplot2	Wickham (2016)	https://ggplot2.tidyverse.org

REAGENT or RESOURCE	SOURCE	IDENTIFIER
R (version 4.0.3)	R core team, 2020	https://www.r-project.org
RStudio	RStudio team, 2020	https://www.rstudio.com
ZEN 2 slidescan	Carl Zeiss AG	https://www.zeiss.com/corporate/int/home.html
Leica LAS X	Leica Biosystems	https://www.leica-microsystems.com/products/microscope-software/p/leica-las-x-ls/

Author Manuscript

Author Manuscript

Author Manuscript

Author Manuscript